tomography revealed muscle atrophy in the bilateral lower legs (Fig. 1B). Sural nerve biopsy revealed a moderate decrease in myelinated fiber density, predominantly large myelinated fibers (3410 fibers/mm^2), axonal atrophy, and redundant myelin loops (Fig. 1C). We did not detect vasculitis or infiltration of inflammatory cells, or amyloid deposition in the endoneurium, which would have been be revealed by Congo red staining. The frequency of segmental demyelination and tomacula in teased-fiber preparations was 12.5% and 10.8%, respectively (Fig. 1D). Widely spaced myelin (WSM) was detected by electron microscopy, and the frequency of one in the myelinated fibers was 17.2% (Fig. 1E). Indirect immunofluorescence for human IgM antibody was positive on myelinated fibers (Fig. 1F).

Based on the laboratory, electrophysiological, and pathological findings, we diagnosed our patient with anti-MAG neuropathy. He was treated with intravenous immunoglobulin (IVIg) therapy and showed clinical improvement. Although he could not remain standing without support prior to IVIg therapy, he was able to walk with a cane thereafter.

DISCUSSION

In this case report we have presented a patient with anti-MAG neuropathy that manifested predominant muscle weakness and extensive muscle atrophy of the lower legs, which is a rare form in this neuropathy. Although muscle weakness is often observed in the distal portion of the lower limbs in patients with anti-MAG neuropathy, it rarely overshadows the sensory features and gait disturbance usually dependent on the sensory ataxia.[8,9,12] Sensorimotor neuropathy with severe weakness in the presence of IgM MGUS was described by Ellie et al.[7] However, all of their patients had severe sensory ataxia and a high ataxic score in addition to muscle weakness, whereas the impairment of deep sensation in our case was mild. Predominant motor symptoms may characterize the features of CMT, chronic inflammatory demyelinating polyradiculoneuropathy (CIDP), and lumbosacral plexopathy. The characteristic features of nerve conduction studies in anti-MAG neuropathy include marked prolongation of distal motor latencies disproportionate to proximal segment conduction velocities, indicating predominantly distal demyelination in contrast to CIDP and CMT.[13] In addition, muscle atrophy was observed in the distal, but not proximal, portion of the lower extremities, and painful symptoms were also not reported. These findings are atypical in lumbosacral plexopathy.[14] Pathological findings further support the view that the pathogenesis of neuropathy in this patient was due to IgM monoclonal gammopathy for the antibody against MAG/SGPG.

Previous reports have revealed that the IgM from patients with neuropathy associated with IgM monoclonal gammopathy could recognize a shared epitope between MAG and glycoconjugates such as SGPG.[10,15] Cross-reactivity between anti-MAG antibody with HNK-1 epitope and other glycoconjugates may be responsible for wide immunoreactivity and may be the reason for the differing clinical manifestations. Predominant motor symptoms and muscle atrophy can be one of the clinical manifestations of anti-MAG neuropathy. Consequently, careful differential diagnosis is necessary for patients with predominant motor neuropathy, especially those with IgM monoclonal gammopathy.

REFERENCES

1. Martini R, Schachner M. Molecular bases of myelin formation as revealed by investigations on mice deficient in glial cell surface molecules. Glia 1997;19:298–310.
2. Lopate G, Kornberg AJ, Yue J, Choksi R, Pestronk A. Anti-myelin associated glycoprotein antibodies: variability in patterns of IgM binding to peripheral nerve. J Neurol Sci 2001;188:67–72.
3. Lunn MP, Crawford TO, Hughes RA, Griffin JW, Sheikh KA. Anti-myelin-associated glycoprotein antibodies alter neurofilament spacing. Brain 2002;125:904–911.
4. Latov N. Pathogenesis and therapy of neuropathies associated with monoclonal gammopathies. Ann Neurol 1995;37(suppl):S32–42.
5. Mendell JR, Sahenk Z, Whitaker JN, Trapp BD, Yates AJ, Griggs RC, et al. Polyneuropathy and IgM monoclonal gammopathy: studies on the pathogenetic role of anti-myelin-associated glycoprotein antibody. Ann Neurol 1985;17:243–254.
6. Vital A, Vital C, Julien J, Baquey A, Steck AJ. Polyneuropathy associated with IgM monoclonal gammopathy. Immunological and pathological study in 31 patients. Acta Neuropathol 1989;79:160–167.
7. Ellie E, Vital A, Steck A, Boiron JM, Vital C, Julien J. Neuropathy associated with "benign" anti-myelin-associated glycoprotein IgM gammopathy: clinical, immunological, neurophysiological and pathological findings and response to treatment in 33 cases. J Neurol 1996;243:34–43.
8. Chassande B, Léger JM, Younes-Chennoufi AB, Bengoufa D, Maisonobe T, Bouche P, et al. Peripheral neuropathy associated with IgM monoclonal gammopathy: correlations between M-protein antibody activity and clinical/electrophysiological features in 40 cases. Muscle Nerve 1998;21:55–62.
9. Nobile-Orazio E, Manfredini E, Carpo M, Meucci N, Monaco S, Ferrari S, et al. Frequency and clinical correlates of anti-neural IgM antibodies in neuropathy associated with IgM monoclonal gammopathy. Ann Neurol 1994;36:416–424.
10. Kusunoki S, Craft JE, Roach B, Hardin JA, Yu RK. Neuropathy and IgM paraproteinemia: differential binding of IgM M-proteins to peripheral nerve glycolipids. Neurology 1987;37:1795–1797.
11. Kusunoki S, Chiba A, Kon K, Ando S, Arisawa K, Tate A, et al. N-acetylgalactosaminyl GD1a is a target molecule for serum antibody in Guillain–Barré syndrome. Ann Neurol 1994;35:570–576.
12. Yeung KB, Thomas PK, King RH, Waddy H, Will RG, Hughes RA, et al. The clinical spectrum of peripheral neuropathies associated with benign monoclonal IgM, IgG and IgA paraproteinaemia. Comparative clinical, immunological and nerve biopsy findings. J Neurol 1991;238:383–391.
13. Kaku DA, England JD, Sumner AJ. Distal accentuation of conduction slowing in polyneuropathy associated with antibodies to myelin-associated glycoprotein and sulphated glucuronyl paragloboside. Brain 1994;117:941–947.
14. Dyck PJ, Norell JE, Dyck PJ. Non-diabetic lumbosacral radiculoplexus neuropathy: natural history, outcome and comparison with the diabetic variety. Brain 2001;124:1197–1207.
15. Weiss MD, Dalakas MC, Lauter CJ, Willison HJ, Quarles RH. Variability in the binding of anti-MAG and anti-SGPG antibodies to target antigens in demyelinating neuropathy and IgM paraproteinemia. J Neuroimmunol 1999;95:174–184.

Clinical Neurology and Neurosurgery xxx (2011) xxx–xxx

Contents lists available at ScienceDirect

Clinical Neurology and Neurosurgery

journal homepage: www.elsevier.com/locate/clineuro

Case report

Central nervous system involvement in n-hexane polyneuropathy demonstrated by MRI and proton MR spectroscopy

A. Hashizume[a], H. Koike[a], Y. Kawagashira[a], H. Banno[a,b], K. Suzuki[a], M. Ito[a], M. Katsuno[a,b], H. Watanabe[a], F. Tanaka[a], S. Naganawa[c], R. Kaneko[d], A. Ishii[d], G. Sobue[a,*]

[a] Department of Neurology, Nagoya University Graduate School of Medicine, 65 Tsurumai-cho, Showa-ku, Nagoya 466-8550, Japan
[b] Institute for Advanced Research, Nagoya University, Nagoya, Japan
[c] Department of Radiology, Nagoya University Graduate School of Medicine, Nagoya, Japan
[d] Department of Legal Medicine and Bioethics, Nagoya University Graduate School of Medicine, Nagoya, Japan

ARTICLE INFO

Article history:
Received 31 August 2009
Received in revised form 19 January 2011
Accepted 22 January 2011
Available online xxx

Keywords:
n-Hexane
Polyneuropathy
Central nervous system
Magnetic resonance spectroscopy
Lactate peak

1. Introduction

The organic solvent n-hexane is a well-described causal agent in polyneuropathy. Although most cases of n-hexane polyneuropathy result from industrial exposure to glues containing the chemical, some are caused by addictive inhalation. In abuse cases, neurological manifestations are generally severe because of the high intensity of exposure.

n-Hexane polyneuropathy has two characteristic electrophysiological features: conduction block and conduction slowing. Nerve biopsy specimens show primarily axonal swelling as well as secondary paranodal myelin retraction and myelin thinning, which may underlie the electrophysiological features [1]. In contrast to toluene toxicity, the damage caused by n-hexane has been considered to be mostly restricted to peripheral nerves [2]. Although many cases of peripheral neuropathy due to n-hexane toxicity have been reported, central nervous system (CNS) involvement has not been fully described in humans, although it has been observed in animal models [3]. A previous electrophysiological study suggested the presence of CNS lesions by evoked potential abnormalities [4].

In the present report, we describe a patient with n-hexane polyneuropathy with CNS lesions using magnetic resonance imaging (MRI) and proton magnetic resonance spectroscopy (^{1}H MRS).

2. Case report

A 51-year-old woman complained of difficulty rising up from a seated position and climbing stairs for six months prior to admission to our hospital. Her symptoms gradually worsened until she could not rise up at all for the month before admission. She had no past or family history of neurological disorders. A neurological examination disclosed no impairment of consciousness. Cranial nerves were normal. Severe bilateral muscle weakness was present. Her grip power was almost zero in both hands. Although touch, pain, and temperature sensations were nearly normal objectively, she felt discomfort described as "walking on sand" on the soles of her feet. Vibration sensations in her lower legs were moderately decreased. Deep tendon reflexes were absent in the upper and lower extremities. Plantar responses were flexor on both sides.

All routine hematological, serological and biochemical examinations were normal. Cerebrospinal fluid examination revealed no abnormalities in cell count or protein level, including myelin basic protein and oligoclonal band. A nerve conduction study (NCS) revealed conduction slowing with conduction block in both motor

* Corresponding author. Tel.: +81 52 744 2385; fax: +81 52 744 2384.
E-mail address: sobueg@med.nagoya-u.ac.jp (G. Sobue).

0303-8467/$ – see front matter
doi:10.1016/j.clineuro.2011.01.008

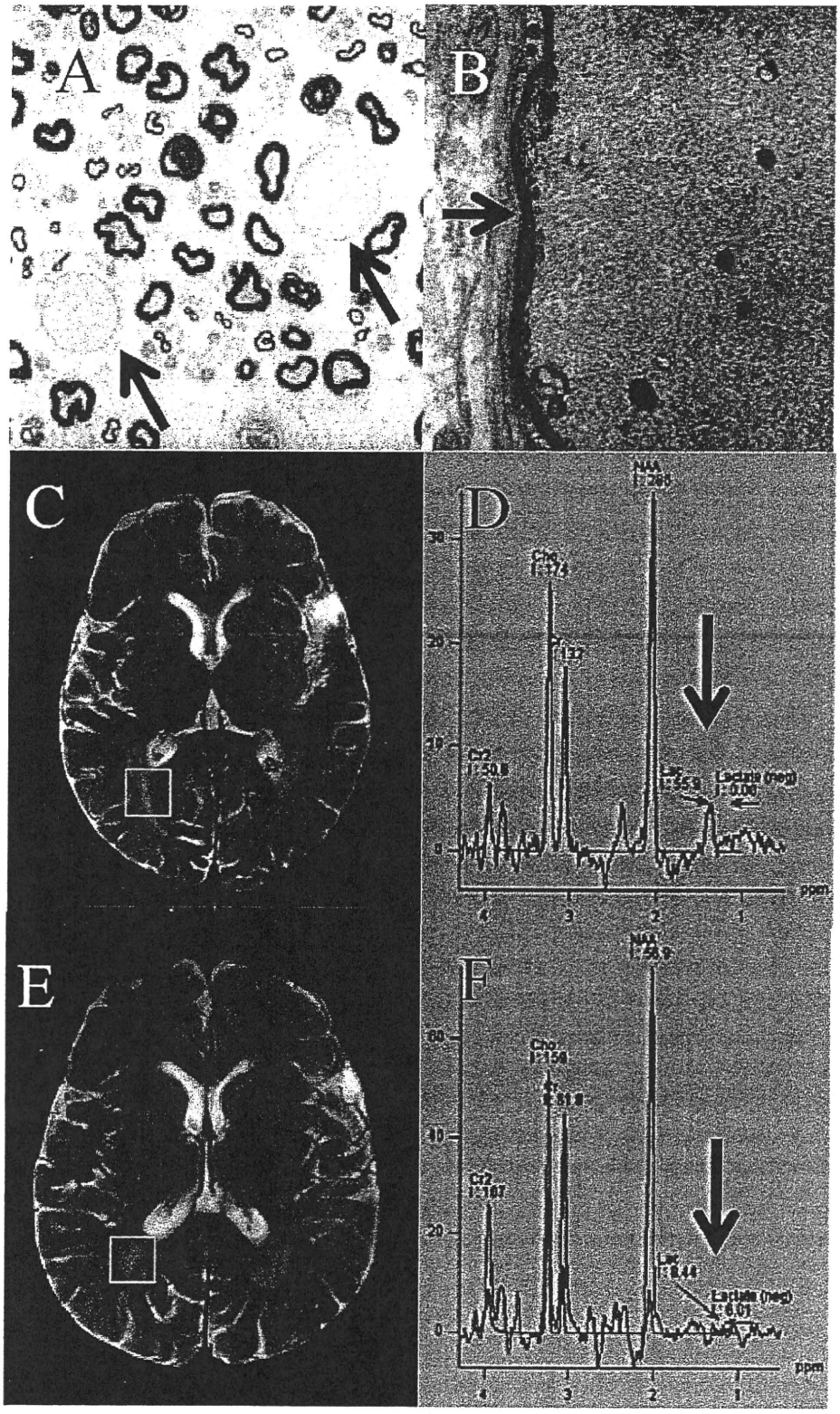

Fig. 1. Sural nerve specimen, head MRI, and proton MR spectroscopy. (A) Light micrograph of transverse section of a sural nerve biopsy specimen showing swollen axons with no or extremely thin myelin (arrow). (B) Electron micrograph showing a giant axon with extremely thin myelin caused by accumulating neurofilaments (arrow). (C) Head T2-weighted MRI image showing a high intensity area of white matter around the cornua of the lateral ventricle. The open white square denotes the region of interest for proton magnetic resonance spectroscopy (^{1}H MRS). (D) ^{1}H MRS showing an abnormal lactate peak (arrow). Although the high intensity area of white matter remained at about the same level (E), the abnormal lactate peak returned to normal in the ^{1}H MRS (F).

Please cite this article in press as: Hashizume A, et al. Central nervous system involvement in n-hexane polyneuropathy demonstrated by MRI and proton MR spectroscopy. Clin Neurol Neurosurg (2011), doi:10.1016/j.clineuro.2011.01.008

and sensory nerves. The compound muscle potential (CMAP), the distal latency (DL), and the motor conduction velocity (MCV) on tibial nerve were 0.6 mV, 10 ms, and 25 m/s, respectively. Sural nerve response could not be elicited. Electromyograms of left tibialis anterior muscle revealed many polyphasic and long duration waveforms. No abnormalities were detected in cervical, thoracic, and lumbar MRI scans.

A nerve biopsy was performed on the left sural nerve. A transverse section of the specimen showed conspicuously swollen axons (Fig. 1A). Although a light microscopic examination did not show any myelin on these swollen axons, electron micrographs revealed an extremely thin myelin layer (Fig. 1B). In addition, a marked accumulation of neurofilaments was observed in the axons. Teased fibers also showed axonal swelling with demyelination or extremely thin myelin. Based on these clinical, electrophysiological, and nerve pathological findings, we suspected the patient as having n-hexane polyneuropathy.

A careful interview with the patient revealed that she bought large amounts of stain remover that contained n-hexane and its isomer (n-hexane 62%, isohexane 25%, metylcyclopentane 13%, others <1%). She had inhaled the solvent addictively for numerous years. She used no other organic solvents. The result of gas chromatograph/mass spectrometry (GC/MS) showed no detectable level of toluene or ethylbenzene.

The patient then underwent cranial MRI and single-voxel ^{1}H MRS on a 1.5-T system (General Electric Signa Infinity HiSpeed SR77, Block Imaging International, Lansing, MI, USA), equipped with a circularly polarized head coil. The MRI protocol included sagittal T1-weighted fluid attenuated inversion recovery (FLAIR; TR, 10,000 ms; TI, 560 ms; TE, 85 ms) and axial T2-weighted fast spin echo (FSE; TR, 4250 ms; TE, 190 ms; ETL, 24 ms) images. Slice thickness was 4 mm, field of view was 24 cm × 24 cm, and matrix size was 320 × 256. ^{1}H MR spectroscopy provided spectra peak areas at 2.0, 3.0, and 3.2 ppm, corresponding to n-acetylaspartate (NAA), creatine (Cr), and choline (Cho). The NAA/Cr, NAA/Cho, and Cho/Cr ratios were analyzed using SAGE (GE Medical Systems, Waukesha, WI, USA). Brain MRI T2-weighted images revealed a high intensity area of white matter around the cornua of the lateral ventricle (Fig. 1C). ^{1}H MRS demonstrated a significant increase in the lactate peak (Fig. 1D). In a brainstem auditory evoked potential (BAEP) study, absolute latencies of I, III, and V were 1.66 ms, 4.16 ms, and 6.36 ms, respectively (normal values [mean ± SD]: 1.7 ± 0.15, 3.9 ± 0.19, and 5.7 ± 0.25, respectively). Thus, the I–III, III–V, and I–V interpeak latencies were 2.50 ms, 2.20 ms, and 4.70 ms, respectively (normal values: 2.1 ± 0.15, 1.9 ± 0.18, and 4.0 ± 0.23, respectively). In a visual evoked potentials (VEPs) study, right and left P100 latency were also prolonged to 122 ms and 117 ms, respectively (normal values: 102.3 ± 5.1). Central nervous conduction times calculated by these results were mildly prolonged.

With no treatment, the patient's muscle strength gradually improved after admission. One month later, she could rise up by herself and her grip power recovered to 5–10 kg W. Although the discomfort in her soles continued to worsen for two more months, it began to improve thereafter. Six months later, the deep tendon reflexes in her lower extremities returned to the normal range. The NCS findings also gradually recovered. CMAP, DL, and MCV on tibial nerve of 10 months after cessation of inhalation were 6.6 mV, 5.0 ms, and 35 m/s, respectively. The sensory nerve action potential and the sensory conduction velocity of sural nerve were 10.1 μV and 44 m/s, respectively. Although the high intensity area of white matter seen in the brain MRI T2-weighted images remained at about the same level six months later (Fig. 1E), the abnormal lactate peak returned to almost normal in the ^{1}H MRS during the clinical discovery (Fig. 1F).

3. Discussion

In this report, we described a patient with a CNS lesion probably due to n-hexane polyneuropathy. The axonal swelling seen in the sural nerve biopsy specimen, the characteristic nerve conduction studies showing both conduction block and conduction slowing, and the improvement of symptoms upon cessation of inhalation, all point to addictive inhalation of n-hexane as the cause of this patient's polyneuropathy. The CNS lesion demonstrated by ^{1}H MRS also showed clear improvement after n-hexane inhalation was stopped. The use of other organic solvents such as toluene, which can induce CNS lesions, was ruled out based on the GC/MS results.

The most striking aspect of this case was the CNS involvement. The cerebral MRI T2-weighted images showed an abnormally high-intensity area around the lateral ventricle. In addition, ^{1}H MRS revealed abnormal, but reversible, lactate peaks. Multiple sclerosis and age-related factors should be considered in the differential diagnosis. However, the patient did not show an elevation of myelin basic protein or oligoclonal band in the cerebrospinal fluid or in any MRI findings in the spinal cord. In addition, an increase in the Cho/Cr ratio or the presence of a lactate peak has not been reported to occur in the white matter of the ageing brain. For these reasons, we conclude that the observed CNS changes were due to n-hexane. The fact that six months after ceasing n-hexane inhalation, the abnormal lactate peaks disappeared strongly supports this conclusion.

Several other reports have suggested CNS effects due to n-hexane inhalation. Oge et al. described a central nerve conduction delay using the electrophysiological method of transcranial magnetic stimulation [5]. Moreover, studies using patterned visual evoked potential (pVEP), brainstem auditory evoked potential (BAEP), and somatosensory evoked potential (SEP) have suggested subclinical central nerve involvement in n-hexane neuropathy [2]. They concluded that there were chronic neurotoxic effects of n-hexane on the CNS, including the cerebrum, the brainstem, and the spinal cord. In addition, Spencer et al. demonstrated a pathological change in the CNS in experimental animals [3]. They reported that light microscopic observation of CNS tissue obtained from rats and cats revealed abnormally large fibers with swollen axons and myelin sheaths inappropriately thin for their diameter. If similar pathological change occurred in the CNS of our patient, the CNS findings demonstrated by MRI or MR spectroscopy we obtained were explainable.

The present case study represents a new line of evidence of CNS involvement in n-hexane polyneuropathy.

References

[1] Kuwabara S, Kai MR, Nagase H, Hattori T. n-Hexane neuropathy caused by addictive inhalation: clinical and electrophysiological features. Eur Neurol 1999;41:163–7.
[2] Chang AP, England JD, Garcia CA, Sumner AJ. Focal conduction block in n-hexane polyneuropathy. Muscle Nerve 1998;21:964–9.
[3] Spencer PS, Schaumburg HH. Ultrastructual studies of the dying-back process. Differential vulnerabilities of PNS and CNS fibers in experimental central–peripheral distal axonopathies. Neuropathol Exp Neurol 1977;36:300–20.
[4] Chang YC. Neurotoxic effects of n-hexane on the human central nervous system: evoked potential abnormalities in n-hexane polyneuropathy. J Neurol Neurosurg Psychiatry 1987;50:269–74.
[5] Oge AM, Yazici J, Boyaciyan A, Eryildiz D, Ornek I, Konyalioglu R, et al. Peripheral and central conduction in n-hexane polyneuropathy. Muscle Nerve 1994;17:1416–30.

Please cite this article in press as: Hashizume A, et al. Central nervous system involvement in n-hexane polyneuropathy demonstrated by MRI and proton MR spectroscopy. Clin Neurol Neurosurg (2011), doi:10.1016/j.clineuro.2011.01.008

Skin biopsy is useful for the antemortem diagnosis of neuronal intranuclear inclusion disease

J. Sone, MD, PhD
F. Tanaka, MD, PhD
H. Koike, MD, PhD
A. Inukai, MD, PhD
M. Katsuno, MD, PhD
M. Yoshida, MD, PhD
H. Watanabe, MD, PhD
G. Sobue, MD, PhD

Address correspondence and reprint requests to Dr. Fumiaki Tanaka, Department of Neurology, Nagoya University Graduate School of Medicine, 65, Tsurumai-cho, Shouwa-ku, Nagoya, Aichi 466-8550, Japan
ftanaka@med.nagoya-u.ac.jp

ABSTRACT

Background: Neuronal intranuclear inclusion disease (NIID) is a progressive neurodegenerative disease characterized by eosinophilic hyaline intranuclear inclusions in neuronal and somatic cells. Because of the variety of clinical manifestations, antemortem diagnosis of NIID is difficult.

Methods: Seven skin biopsy samples from patients with familial NIID were evaluated histochemically, and the results were compared with those of skin samples from normal control subjects and from patients with other neurologic diseases. We also examined skin biopsy samples from patients with NIID by electron microscopy.

Results: In NIID skin biopsy samples, intranuclear inclusions were observed in adipocytes, fibroblasts, and sweat gland cells. These inclusions were stained with both anti-ubiquitin and anti-SUMO1 antibodies. Electron microscopy revealed that the features of the intranuclear inclusions in adipocytes, fibroblasts, and sweat gland cells were identical to those of neuronal cells. Approximately 10% of adipocytes showed intranuclear inclusions. No intranuclear inclusions were identified in the skin samples from normal control subjects and patients with other neurologic diseases.

Conclusions: Skin biopsy is an effective and less invasive antemortem diagnostic tool for NIID.

Neurology® 2011;76:1372–1376

GLOSSARY

ALS = amyotrophic lateral sclerosis; **CMT** = Charcot-Marie-Tooth; **DAPI** = 4′,6-diamidino-2-phenyindole di-lactate; **DRPLA** = dentatorubral pallidoluysian atrophy; **FAP** = familial amyloid polyneuropathy; **HD** = Huntington disease; **H&E** = hematoxylin & eosin; **MSA** = multiple system atrophy; **NIID** = neuronal intranuclear inclusion disease; **PD** = Parkinson disease; **PSP** = progressive supranuclear palsy; **SBMA** = spinal and bulbar muscular atrophy; **SCA3** = spinocerebellar ataxia 3.

Neuronal intranuclear inclusion disease (NIID), also known as neuronal intranuclear hyaline inclusion disease, is a progressive neurodegenerative disease characterized by eosinophilic hyaline intranuclear inclusions in neuronal and visceral organ cells.[1-4] Clinical manifestations of NIID are highly variable and can include pyramidal and extrapyramidal symptoms, cerebellar ataxia, dementia, convulsion, neuropathy, and autonomic dysfunction.[1-6] Both sporadic and familial cases have been reported, and the onset of disease varies from infantile stages to late middle age.[1-6] The antemortem diagnosis of NIID is difficult, and most of the reported cases of NIID are diagnosed by postmortem histopathologic examination. Some reports have described antemortem diagnosis of NIID by rectal biopsy[5,6] and sural nerve biopsy.[2] However, rectal biopsy has a risk of perforation,[7] and sural nerve biopsy is applicable only in patients with sensory disturbance.[2] To avoid the difficulty of antemortem diagnosis of NIID by rectal or sural nerve biopsy, we investigated skin biopsy samples from patients with familial NIID and compared the findings with those of samples from normal control subjects and from patients with other neurodegenerative diseases. Our results suggest that skin biopsy is a useful and safe tool for the antemortem diagnosis of NIID.

Editorial, page 1368

e-Pub ahead of print on March 16, 2011, at www.neurology.org.

From the Department of Neurology (J.S., F.T., H.K., H.W., G.S.), Nagoya University Graduate School of Medicine, Nagoya; Department of Neurology (A.I.), National Hospital Organization Higashi Nagoya National Hospital, Nagoya; Institute for Advanced Research (M.K.), Nagoya University, Nagoya; and Department of Neuropathology (M.Y.), Institute for Medical Sciences of Aging, Aichi Medical University, Aichi, Japan.

Study funding: Supported by a 21st Century Center of Excellence (COE) grant and a global COE grant from the Ministry of Education, Culture, Sports, Science and Technology of Japan and by a grant from the Ministry of Health, Welfare and Labor of Japan.

Disclosure: Author disclosures are provided at the end of the article.

METHODS Subjects. Skin tissue samples were collected from autopsy samples, and skin biopsy samples were collected from patients at Nagoya University Hospital and from normal volunteers. Overall, skin biopsy samples from 7 patients with familial NIID from 2 pedigrees, as we reported previously,[2] were analyzed. Patients with sporadic NIID were not included. For other neurodegenerative diseases, 3 biopsy samples from patients with Charcot-Marie-Tooth (CMT) disease with *PMP22* duplication, 2 autopsy samples and one biopsy sample from patients with familial amyloid polyneuropathy (FAP), one biopsy sample from a patient with genetically diagnosed Huntington disease (HD), 3 biopsy samples from patients with spinocerebellar ataxia 3 (SCA3), 3 biopsy samples from patients with dentatorubral pallidoluysian atrophy (DRPLA), 2 autopsy samples and one biopsy sample from patients with spinal and bulbar muscular atrophy (SBMA), 3 autopsy samples from patients with sporadic amyotrophic lateral sclerosis (ALS), 2 autopsy samples and one biopsy sample from patients with Parkinson disease (PD), one autopsy sample and 2 biopsy samples from patients with multiple system atrophy (MSA), 2 autopsy samples and one biopsy sample from patients with progressive supranuclear palsy (PSP), and 8 samples from normal volunteers were analyzed. All the patients with CMT, FAP, SCA3, DRPLA, and SBMA were assessed genetically.

Standard protocol approvals, registrations, and patient consent. The study was performed with approved protocols and informed consent in accordance with the institutional review board of Nagoya University School of Medicine. Written informed consent was obtained from all patients and normal volunteers.

Skin biopsy, immunohistochemistry, and electron microscopic study. After local anesthesia, a 3-mm-diameter punch biopsy specimen was obtained at 10 cm above the lateral malleolus. All samples were fixed in 10% formalin. Sections of all samples (4 μm) were stained by hematoxylin & eosin (H&E), and immunohistochemical analysis was performed using a Ventana DISCOVERY system (Ventana Medical Systems, Tucson, AZ). Sections were incubated with anti-ubiquitin antibody (Z0458; DAKO, Glostrup, Denmark) and anti-SUMO1 antibody (sc-5308; Santa Cruz Biotechnology, Santa Cruz, CA) using the Ventana DAB Map kit. For immunofluorescence staining, sections were blocked with 4% goat serum and incubated in anti-ubiquitin antibody (P4D1; Santa Cruz Biotechnology). Bound anti-ubiquitin antibody was visualized using antimouse goat immunoglobulin G coupled with Alexa Fluor 488 (Molecular Probes, Eugene, OR). Nuclei were stained with 1.5 μg/mL 4′,6-diamidino-2-phenyindole di-lactate (DAPI). Samples for electron microscopy were fixed in glutaraldehyde in cacodylate buffer and embedded in epoxy resin.[8]

RESULTS We performed more than 30 skin biopsies with no adverse reaction or accident. H&E-stained sections from patients with NIID demonstrated eosinophilic intranuclear inclusions in adipocytes, fibroblasts, and sweat gland cells in the dermis (figure 1, A–C). The nuclei of these cells were strongly stained basophilic, which made it difficult to observe inclusions in such small, dark-stained nuclei (figure 1, A–C). In anti-ubiquitin-stained sections using the DAB technique (figure 1, D–F), intranuclear inclusions were identified easily in all 7 NIID samples. However, erythrocytes and some secreted materials from the sweat glands were strongly stained with the anti-ubiquitin antibody, which made it difficult to distinguish these materials from intranuclear inclusions.

By examination using electron microscopy, intranuclear inclusions in adipocytes, fibroblasts, and sweat gland cells showed common features (figure 1, G–L). These inclusions were composed of filamentous material and showed no limiting membrane. The nuclei of adipocytes were observed as entirely electron dense, but we were able to identify inclusions in the nuclei of adipocytes (figure 1, G and J). The nuclei of fibroblasts were less electron dense than those of adipocytes, and inclusions were recognized easily as electron-dense spherical bodies and filaments arranged in turbinate fashion (figure 1, H and K). In the sweat gland cells, intranuclear inclusions were observed as electron light material in the nucleus (figure 1, I and L).

We also examined anti-SUMO1 antibody immunoreactivity. SUMO1 is a small ubiquitin-like modifier protein that covalently conjugates to various intracellular target proteins to alter their cellular distribution, function, and metabolism. Neuronal intranuclear inclusions of patients with NIID are immunoreactive for SUMO1.[9] Intranuclear inclusions in the dermal cells showed anti-SUMO1 immunoreactivity (figure 1, M–O), similar to results previously reported for NIID neuronal cells.[1,9]

These features of inclusions are identical to those of neuronal inclusions in patients with NIID (figure 1, P–T).[2]

Frequency of intranuclear inclusions. We investigated the frequency of intranuclear inclusions in adipocytes, fibroblasts, and sweat gland cells using anti-ubiquitin antibody and DAPI for the purpose of distinguishing intranuclear inclusions from other ubiquitin-positive materials. Intranuclear inclusions were recognized readily as ubiquitin-positive inclusions within DAPI-positive nuclei under merge view (figure 2A). The frequency of intranuclear inclusion–positive adipocytes in NIID skin samples was approximately 10%, which represented the highest frequency among the 3 cell types (table).

Immunofluorescence examination in NIID and a wide range of neurodegenerative diseases. To examine the specificity of skin biopsy for the diagnosis of NIID, we investigated adipocytes in sections of skin samples from patients with NIID and other neurodegenerative diseases that were double-stained with anti-ubiquitin antibody and DAPI (figure 2, A and B). Intranuclear inclusions were not observed in normal control samples (figure 2C). No inclusions were observed in adipocytes from patients with CMT disease and FAP, who show clinical symptoms similar to

Figure 1 Histopathologic features of neuronal intranuclear inclusion disease (NIID) cells

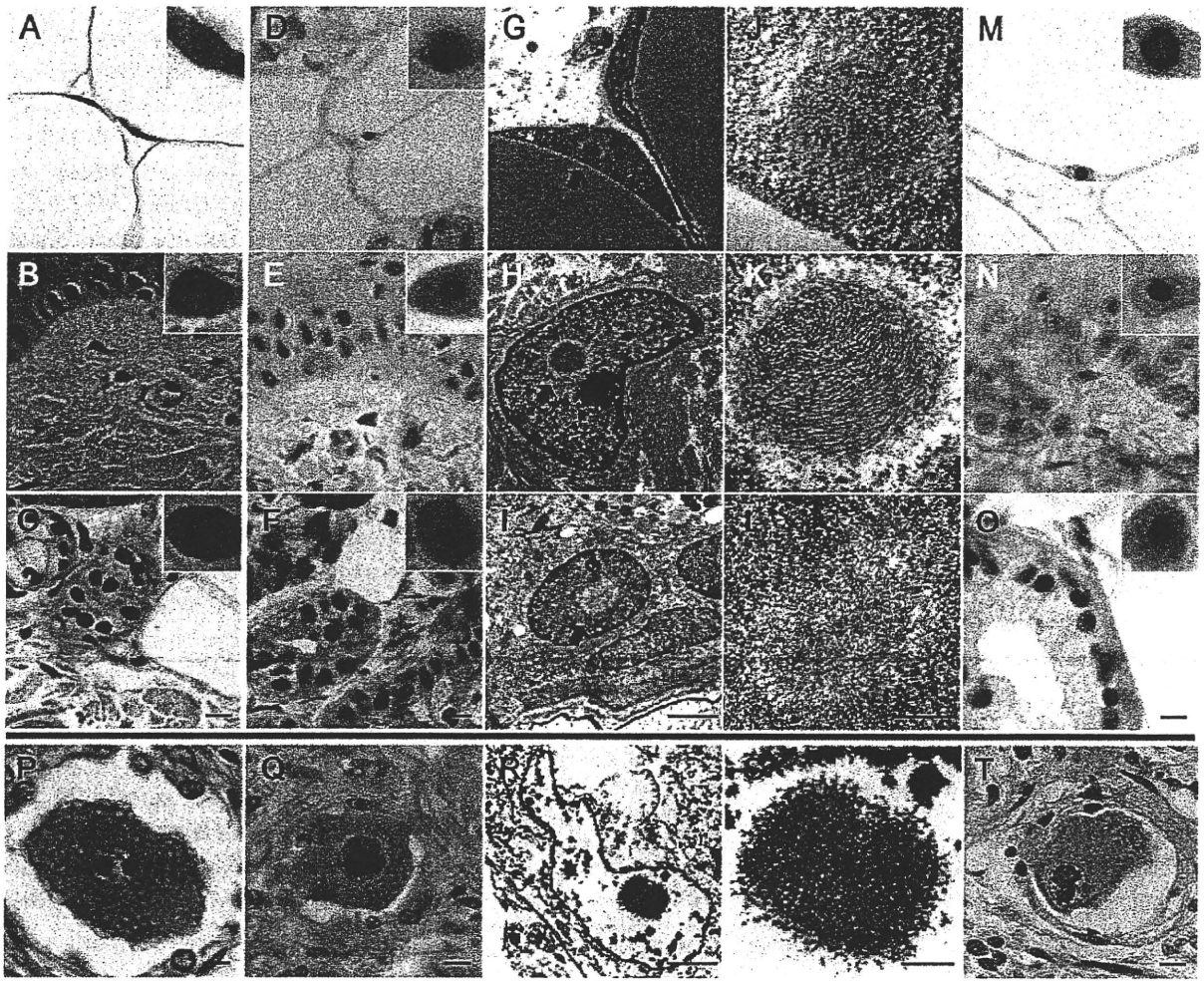

(A–C) Hematoxylin & eosin (H&E) stain of adipocytes (A), fibroblasts (B), and sweat gland cells (C). (D–F) Immunostained samples of adipocytes (D), fibroblasts (E), and sweat gland cells (F) with anti-ubiquitin antibody using the DAB technique. (G–L) Electron microscopic images of adipocytes (G, J), fibroblasts (H, K), and sweat gland cells (I, L). (G–I) Lower magnification view of intranuclear inclusion (arrow). (J–L) Higher magnification view of each intranuclear inclusion. (M–O) Immunostaining with anti-SUMO1 antibody using the DAB technique of adipocytes (M), fibroblasts (N), and sweat gland cells (O). (P–T) Histopathologic features of intranuclear inclusion of neuronal cells of patients with NIID[2]: H&E stain of sympathetic ganglion neuron (P); immunostaining with anti-ubiquitin antibody of dorsal root ganglion neuron (Q); electron microscopic images of astrocyte of anterior horn in lower magnification (R) and higher magnification (S); and immunostaining with anti-SUMO1 antibody of sympathetic ganglion neuron (T). (A–F, M–Q, T) Scale bar = 10 μm. (G–I, R) Scale bar = 2.0 μm. (J–L, S) Scale bar = 500 nm.

those of patients with NIID[2] (figure 2, D and E), or in patients with triplet-repeat diseases (HD, SCA3, DRPLA, and SBMA), ALS, PD, MSA, or PSP (figure 2, F–M). No intranuclear inclusions were observed in fibroblasts and sweat gland cells from normal control subjects and from patients with other neurologic diseases (data not shown).

DISCUSSION In H&E-stained sections from patients with familial NIID, we observed intranuclear inclusions in adipocytes, fibroblasts, and sweat gland cells, but difficulty in observing the inclusions was encountered because of the size and density of the nuclei. Immunohistochemical analysis using anti-ubiquitin antibody with a DAB-based technique revealed intranuclear inclusions more distinctly than H&E staining. These results suggest that double fluorescence staining with anti-ubiquitin antibody and DAPI is a more reliable method to detect intranuclear inclusions in skin samples from patients with NIID, and we recommend this method for the diagnosis of NIID.

Intranuclear inclusions detected in adipocytes, fibroblasts, and sweat gland cells in skin samples were visible in H&E-stained sections, were positive for anti-ubiquitin antibody and anti-SUMO1 antibody, and showed filamentous materials and no limiting membrane. These features of inclusions are identical to those reported for NIID inclusions in neuronal

Figure 2 **Immunofluorescence examination of skin samples from patients with neuronal intranuclear inclusion disease (NIID) and other neurodegenerative diseases**

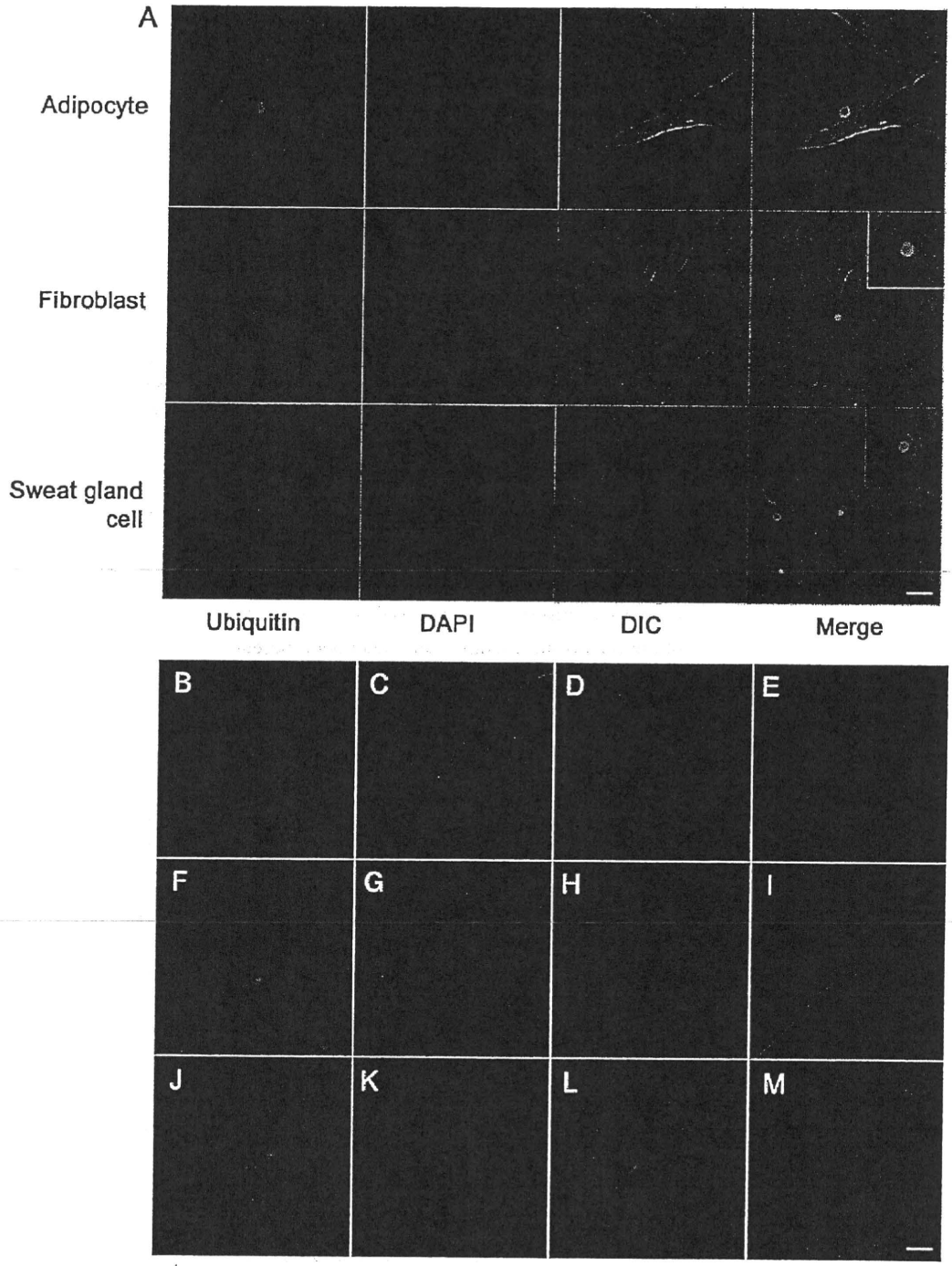

(A) Double immunofluorescence staining with anti-ubiquitin antibody and 4′,6-diamidino-2-phenyindole di-lactate (DAPI) in NIID skin samples from family I.[2] Intranuclear inclusions were stained with anti-ubiquitin antibody (green) and these inclusions are included in the DAPI-positive nuclei in the merged view. Scale bar = 10 μm. (B–M) Double fluorescence staining for adipocytes in dermis with anti-ubiquitin antibody and DAPI in NIID family II[2] (B), normal control (C), Charcot-Marie-Tooth disease (D), familial amyloid polyneuropathy (E), Huntington disease (F), spinocerebellar ataxia 3 (G), dentatorubral pallidoluysian atrophy (H), spinal and bulbar muscular atrophy (I), amyotrophic lateral sclerosis (J), Parkinson disease (K), multiple system atrophy (L), and progressive supranuclear palsy (M). Scale bars = 10 μm.

Table Frequency of intranuclear inclusions in adipocytes, fibroblasts, and sweat gland cells in patients with NIID[a]

	Adipocytes			Fibroblasts			Sweat gland cells		
Patients	No. of nuclei	No. of inclusions	% Inclusion + nuclei	No. of nuclei	No. of inclusions	% Inclusion + nuclei	No. of nuclei	No. of inclusions	% Inclusion + nuclei
1	204	15	7.4	493	33	6.7	366	13	3.6
2	188	19	10.1	391	18	4.6	195	11	5.6
3	44	7	15.9	215	30	14	111	8	7.2
4	38	5	13.2	456	29	6.4	290	12	4.1
5	59	7	11.9	287	22	7.7	318	14	4.4
6	103	9	8.7	427	37	8.7	91	6	6.6
7	138	12	8.7	397	40	10.1	243	7	2.9
Average ± SD			10.8 ± 3.0			8.3 ± 3.1			4.9 ± 1.6

Abbreviations: DAPI = 4′,6-diamidino-2-phenyindole di-lactate; NIID = neuronal intranuclear inclusion disease.
[a] All patients had familial NIID and were from 2 NIID families that we reported previously.[2] The number of nuclei of each cell type was counted as DAPI-positive nuclei under double immunofluorescence staining. The number of intranuclear inclusions was counted in a merged view of ubiquitin immunofluorescence and DAPI staining (figure 2A).

cells (figure 1).[1-4,9] We suggest that the intranuclear inclusions in dermal cells have a pathologic background similar to that of neuronal cells and are useful for NIID diagnosis. Furthermore, because no intranuclear inclusions were observed in dermal cells from normal control samples and other neurodegenerative disease skin samples, skin biopsy is a powerful tool for the differential diagnosis of NIID from other neurologic diseases.

The examination of a few slides of double-immunostained skin samples may be sufficient for the diagnosis of NIID because the frequency of intranuclear inclusions in adipocytes was approximately 10%. Skin biopsy is an accepted and established technique.[10] It requires only local anesthesia and is safer and easier and presents less stress to patients than rectal biopsy or sural nerve biopsy. Taken together, our results suggest that skin biopsy is an acceptable and less invasive tool for the antemortem diagnosis of NIID.

DISCLOSURE

Dr. Sone reports no disclosures. Dr. Tanaka has received research support from the Grants-in-Aid for Scientific Research from the Ministry of Education, Culture, Sports, Science and Technology of Japan (21659221, 22390175), and a grant from the Ministry of Health, Welfare and Labor of Japan. Dr. Koike has received research support from the Grants-in-Aid for Scientific Research from the Ministry of Education, Culture, Sports, Science and Technology of Japan (21591076), and a grant from the Ministry of Health, Welfare and Labor of Japan. Dr. Inukai reports no disclosures. Dr. Katsuno received research support from the Grants-in-Aid for Scientific Research from the Ministry of Education, Culture, Sports, Science and Technology of Japan (21689024, 2110005). Dr. Yoshida received research support from the Grants-in-Aid for Scientific Research from the Ministry of Education, Culture, Sports, Science and Technology of Japan (21500339), and a grant from the Ministry of Health, Welfare and Labor of Japan. Dr. Watanabe reports no disclosures. Dr. Sobue serves on scientific advisory boards for Kanae Science Foundation for the Promotion of Medical Science, Naito Science Foundation, and has received research support from the Ministry of Education, Culture, Sports, Science and Technology of Japan (21229011, 17025020, 09042025), the Ministry of Welfare, Health and Labor of Japan, and the Japan Science and Technology Agency, Core Research for Evolutional Science and Technology.

Received August 6, 2010. Accepted in final form November 17, 2010.

REFERENCES

1. Woulfe JM. Abnormalities of the nucleus and nuclear inclusions in neurodegenerative disease: a work in progress. Neuropathol Appl Neurobiol 2007;33:2–42.
2. Sone J, Hishikawa N, Koike H, et al. Neuronal intranuclear hyaline inclusion disease showing motor-sensory and autonomic neuropathy. Neurology 2005;65:1538–1543.
3. Takahashi-Fujigasaki J. Neuronal intranuclear hyaline inclusion disease. Neuropathology 2003;23:351–359.
4. Lindenberg R, Rubinstein LJ, Herman MM, Haydon GB. A light and electron microscopy study of an unusual widespread nuclear inclusion body disease: a possible residuum of an old herpesvirus infection. Acta Neuropathol 1968;10:54–73.
5. Kulikova-Schupak R, Knupp KG, Pascual JM, Chin SS, Kairam R, Patterson MC. Rectal biopsy in the diagnosis of neuronal intranuclear hyaline inclusion disease. J Child Neurol 2004;19:59–62.
6. Zannolli R, Gilman S, Rossi S, et al. Hereditary neuronal intranuclear inclusion disease with autonomic failure and cerebellar degeneration. Arch Neurol 2002;59:1319–1326.
7. Tanaka S, Oka S, Chayama K. Colorectal endoscopic submucosal dissection: present status and future perspective, including its differentiation from endoscopic mucosal resection. J Gastroenterol 2008;43:641–651.
8. Koike H, Iijima M, Mori K, et al. Nonmyelinating Schwann cell involvement with well-preserved unmyelinated axons in Charcot-Marie-Tooth disease type 1A. J Neuropathol Exp Neurol 2007;66:1027–1036.
9. Pountney DL, Huang Y, Burns RJ, et al. SUMO-1 marks the nuclear inclusions in familial neuronal intranuclear inclusion disease. Exp Neurol 2003;184:436–446.
10. Lauria G, Cornblath DR, Johansson O, et al. EFNS guidelines on the use of skin biopsy in the diagnosis of peripheral neuropathy. Eur J Neurol 2005;12:747–758.

(会)

シャルコー―マリー―トゥース病患者診療の現況 全国1次アンケート調査報告*

滋賀　健介, 中川　正法

Peripheral Nerve 2010; 21(2): 360–361

目　的

シャルコー・マリー・トゥース病（CMT）は進行性の遺伝性ニューロパチーであるが、現在特定疾患に認定されていないため、わが国での診療実態についてのまとまった報告は少ない。その一方で、医療施設で診療されない患者も存在し、患者の実情把握はきわめて重要である。今回、われわれは全国医療機関へアンケート調査を行い、患者の分布・ADL・装具療法など診療実態の把握を試みたので報告する。

対象・方法

医療機関アンケート：全国の神経内科・小児科・リハビリテーション科（リハ科）の教育関連施設と足の外科学会関連施設あわせて計1,841施設に手紙によるアンケート調査を行い、診療されているCMT患者の数・男女比・ADL・装具療法・手術療法・リハビリテーションなどを受けている患者数・外来診療間隔などを記入形式で回答していただいた（2009年10月実施）。

結　果

全国879施設（47.7%）から回答があり、うち244施設で計509名のCMT患者が診療されていた。1施設で診療されている患者数は1人～22人と幅があったが、3人以上診療している施設は73施設であった。性別では、男性284人、女性225人。年齢別では、10歳未満35人、11歳～20歳：74人、21歳～30歳：54人、31歳～40歳：64人、41歳～50歳：67人、51歳～60歳：91人、60歳以上：124人と11歳～20歳に小さいピークがある以外は、高齢者ほど患者数が多かった（図1A）。整形外科関連施設を除くと11歳～20歳に見られたピークは消失した。患者のADLレベルでは、杖なし歩行が58.5%、杖歩行が21.2%、車椅子が19.3%、寝たきりが1%であった（図1B）。医療処置に関しては、短下肢装具使用が31.6%、長下肢装

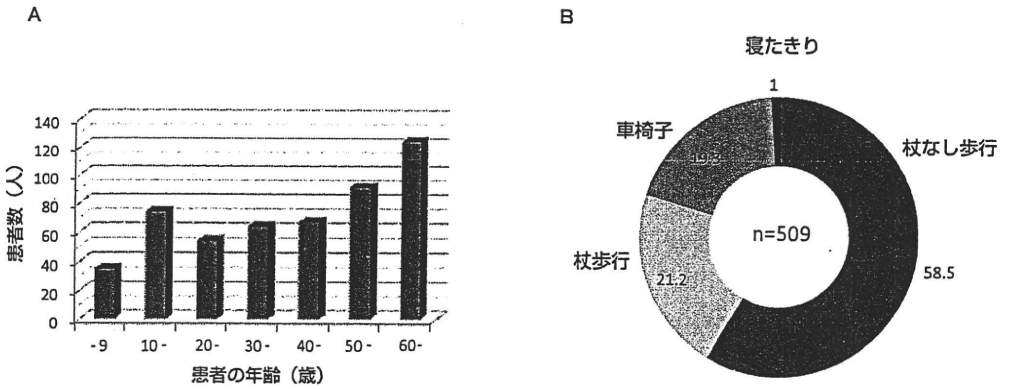

図1　A. 医療機関アンケートによるCMT患者の年齢分布（n = 509）.
B. 医療機関アンケートによるCMT患者のADLレベル（n = 509）. 数は%をしめす.

* A nationwide survey on actual conditions in patients with Charcot Maie-Tooth disease: a preliminary report.

Kensuke SHIGA, M.D.,Ph.D. and Masanori NAKAGAWA, M.D.,Ph.D.：京都府立医科大学神経内科［〒602-8566 京都市上京区梶井町465］：Department of Neurology, Kyoto Prefectural University of Medicine, Kyoto

(会)

右腕神経叢症で発症したneurolymphomatosisの一例*

辻 有希子[1)], 田中 章浩[1)], 諫山 玲名[1)]
笠井 高士[1)], 吉田 誠克[1)], 藤原 康弘[1)]
滋賀 健介[1)], 水野 敏樹[1)], 中川 正法[1)]
松本 洋典[2)]

Peripheral Nerve 2010; 21(2): 353–354

はじめに

Neurolymphomatosisは悪性リンパ腫の中では比較的稀な病態であるが[1),2)]、腕神経叢症を来すものは約40%と報告されている[2)]。今回われわれは腕神経叢症で発症し、電気生理検査で部位診断し、造影MRIとPET-CTで質的診断をしえたneurolymphomatosisの一例を経験したので報告する。

症　例

症例：82歳女性。76歳時にdiffuse large B cell lymphoma（DLBCL）を発症し、80歳時に再発の既往あり。2009年2月、右母指に異常感覚を自覚、1ヵ月後には遠位側優位の右上肢筋力低下が出現し徐々に増悪、4月に疼痛が出現し増悪したため7月入院となった。

入院時現症：右上肢において手内在筋の筋萎縮、短母指外転筋・小指外転筋・手根屈筋・手根伸筋・上腕二頭筋・腕橈骨筋・菱形筋・前鋸筋の筋力低下を認めた。また、右上肢全体に異常知覚、右手掌に感覚低下を認めた。左上肢および両下肢は運動系・感覚系とも正常であった。右上肢腱反射は消失していた。

検査所見：血算、生化学検査は正常、各種自己抗体も陰性であった。血清、髄液ともに抗s-IL2R抗体も陰性で、髄液細胞診はClass Ⅱであった。

電気生理学的所見：右尺骨・正中・橈骨神経にて、CMAPの低下・Erb-腋窩間での伝導ブロックを認め、右腕神経叢病変が推定された。

画像所見：造影MRIで右腕神経叢に造影効果を認める神経肥厚を認めた。FDG-PETで左鼠径部・左膝窩・右神経叢に沿ってhot spotを認めた。

生検：左鼠径部リンパ節生検・左膝窩皮膚生検で、CD20陽性悪性リンパ腫と診断した。

経過：右腕神経叢でのhot spotも同様の病理であると推測し、右上肢の症状はneurolymphomatosisによる腕神経叢症と考えた。2009年7月中旬に血液内科へ転科し、リツキシマブを併用したDeVIC療法を6コース施行した。同年12月にはFDG-PETでhot spotの消失を認め、右上肢の運動・感覚症状と、Erb・腋窩間の伝導ブロックは改善した。

考　察

腕神経叢症のみで発症したneurolymphomatosisは検索した限りでは9例の報告がある[3)-6)]。うち4例がlymphoma初発例で、5例がlymphoma再発例である。また9例のうち2例で両側の腕神経叢症を認めていた。腕神経叢症はneurolymphmatosisのうちでは約40%と決して少なくなく[2)]、腕神経叢症を診断した際にはneurolymphomatosisを鑑別に考える必要がある。

---

* Brachial plexus neurolymphomatosis: A case report.

[1)]Yukiko TSUJI, M.D., Akihiro TANAKA, M.D., Reina ISAYAMA, M.D., Takashi KASAI, M.D., Tomokatsu YOSHIDA, M.D., Yasuhiro FUJIWARA, M.D., Kensuke SHIGA, M.D., Toshiki MIZUNO, M.D. and Masanori NAKAGAWA, M.D.：京都府立医科大学神経内科［〒602-8566 京都市上京区梶井町465］; Department of Neurology, Kyoto Prefectural University of Medicine, Kyoto

[2)]Yosuke MATSUMOTO, M.D.：京都府立医科大学血液内科［〒602-8566 京都市上京区梶井町465］; Department Hematology, Kyoto Prefectural University of Medicine, Kyoto

文　献

1) Kelly J J, Karcher D. Lymphoma and Peripheral Neuropathy: a Clinical Review. *Muscle Nerve* 2005; 31: 301-313.
2) Grisariu S, Avni B, Batchelor T T, *et al.* Neurolymphomatosis: an international Primary CNS Lymphoma Collabrative Group report. *BLOOD* 2010; 17: 5005-5011.
3) Hoshikawa Y, Oguri T, Hattori M, *et al.* A case of neurolymphomatosis diagnosed with FDG-PET. *Rinsho Shinkeigaku* 2007; 47: 437-440.
4) Chamberlain M C, Fink J. Neurolymphomatosis:a rare metastatic complication of diffuse large B-Cell lymphoma. *J Neurooncol* 2009; 95: 285-288.
5) Bokstein F, Goor O, Shihman B, *et al.* Assessment of neurolymphomatosis by brachial plexus biopsy and PET/CT. Report of a case. *J Neurooncol* 2005; 72: 163-167.
6) Swarnkar A, Fukui M B, Fink D J, *et al.* MR Imaging of Brachial Plexopathy in Neurolymphomatosis. *AJR* 1997; 169: 1189-1190.

神経内科，70(4)：354-365，2009

特集 難治性ニューロパチー

Charcot-Marie-Tooth病の遺伝子診断*

髙嶋 博**

Key Words：HMSN, CMT, mutation screening, microarray, re-sequencing array

Charcot-Marie-Tooth病の分類

Charcot-Marie-Tooth病(以下，CMTと略)は，足の変形(凹足)や逆シャンペンボトルと呼ばれる下肢遠位筋萎縮の症状を特徴とする遺伝性の運動・感覚ニューロパチーである．Hereditary motor and sensory neuropathy(HMSN)もほぼ同義語のように用いられているが，CMTイコールHMSNではなく，歴史的な経過が分類に影響を与えている．現在は，遺伝子異常を含めた分類ではCMTが中心に用いられている．

通常，CMTは型別に，CMT1Aというようにに，CMTのあとに数字とアルファベットで記載される．臨床的および遺伝学的にミエリンの障害が主体で優性遺伝形式のものをCMT1，劣性遺伝形式のものをCMT4，軸索の障害によるものをCMT2と分類する．CMTは，臨床的および遺伝的に多くの型に分けられ，少なくとも32の原因遺伝子に加え，8以上の遺伝子座が報告されている(表1)[1]．表のように遺伝子座や原因遺伝子により分類されるが，同じ遺伝子異常でもさまざまな病型を示しうる．脱髄型か軸索型かは正中神経運動神経伝導速度(MCV)38m/secを境に電気生理学的に決定され，それ以下を脱髄型としている．しかし，家系内でMCVが38m/secの上下にまたがる症例/家系もあり，中間的なMCVを呈する型は優性遺伝形式の場合にはdominant intermediate CMT(CMT DIまたはDI-CMT)と呼ばれる．CMTXのMCVの分布もまた中間的な値をとる．

一方，脱髄型においては臨床的に発症年齢や重症度でも分類され，先天性でfloppy infantを呈する最重症型がCHN(congenital hypomyelinating neuropathy)，生後から幼少時期(通常2歳以下)に発症するものをDSS(Dejerine-Sottas syndrome)またはDSN(Dejerine-Sottas neuropathy)，発症の遅いものをCMT1またはCMT4に分類する．圧迫などにより繰り返し起こる脱髄型ニューロパチーはHNPP(hereditary neuropathy with liability to pressure palsies)と呼ばれる．さらに，遺伝子異常，臨床的特徴によりさまざまなサブタイプに分けられる．また，上肢の再発性のplexus neuropathyをひき起こすhereditary neuralgic amyotrophy(HNA)という病型もあり，原因遺伝子*SEPT9*が同定され[2]，本邦での症例も確認されている．

原因遺伝子頻度

アメリカの報告ではあるが，頻度の統計にもっとも影響を与えると思われるコマーシャルの遺伝子検査が開始される前に収集された検体による遺伝子頻度の報告では，もっとも頻度の高いCMTはCMT1Aで常染色体優性遺伝形式(AD)で

* Genetic diagnosis in Charcot-Marie-Tooth disease.

** Hiroshi TAKASHIMA, M.D., Ph.D.: 鹿児島大学大学院医歯学総合研究科神経病学講座神経内科・老年病学分野〔〒890-8520 鹿児島県鹿児島市桜ヶ丘8-35-1〕; Department of Neurology and Geriatrics, Kagoshima University Graduate School of Medical and Dental Sciences, Kagoshima 890-8520, Japan.

表1 遺伝性ニューロパチーの遺伝子座，原因遺伝子と臨床病型

脱髄型	遺伝子	臨床表現型	軸索型	遺伝子	臨床表現型
・常染色体優性			・常染色体優性		
17p11.2-p12	*PMP22*	CMT1A, HNPP, DSS	1p35-p36	*MFN2*	CMT2A2
			1p35-p36	*KIF1B*	CMT2A1
1q22	*MPZ*	CMT1B, DSS, CHN	3q13-q22	*RAB7*	CMT2B
			12q23-q24		CMT2C
16p13	*SIMPLE/LITAF*	CMT1C	7p15	*GARS*	CMT2D, HMN5A, SMAD1
10q21.1-q22.1	*EGR2*	CMT1D, DSS			
8p21	*NEFL*	CMT1F, CMT2E	8p21	*NEFL*	CMT2E, CMT1F
22q13	*SOX10*	CHN	7q11-q21	*HSPB1*	CMT2F, dHMN
8q23-q24	*ARHGEF10*	slowed NCV	12q12		CMT2G
・常染色体劣性			1q22	*MPZ*	CMT2I, CMT2J
8q13-q21.1	*GDAP1*	CMT4A	12q24	*HSPB8*	CMT2L, dHMN 2
11q22.1	*MTMR2*	CMT4B1	7q22		HMSN＋ataxia
11p15	*SBF2/MTMR13*	CMT4B2	・常染色体劣性		
5q23-q33	*KIAA1985*	CMT4C	1q21.2-q21.3	*LMNA*	AR-CMT2A
8q24	*NDRG1*	CMT4D (Lom type)	19q13.3		AR-CMT2B
			8q21.1	*GDAP1*	AR-CMT＋hoarseness, CMT2K
10q21	*EGR2*	CMT4E, CHN			
17p11.2-p12	*PMP22*	CMTIA, CHN, DSS	8q21.3		CMT2H
			16q24.1	*GAN1*	GAN : Giant axonal neuropathy
19q13.13-q13.2	*PRX*	DSS, CMT4F			
10q22-q23		HMSN-Russe (CMT4G)	15q13-q15	*KCC3*	ACCPN, Andermann syndrome
12p11.2-q13.1	*FGD4*	CMT4H	9q13	*APTX*	EAOH, AOA1
6q21	*FIG4*	CMT4J	9q34	*SETX*	AOA2
・X染色体優性			14q31-q32	*TDP1*	SCAN1
Xq13.1	*GJB1*	CMTX1	・X染色体優性		
・CMT(中間型)常染色体優性			Xq13.1	*GJB1*	CMTX1
			・X染色体劣性		CMTX5
10q24.1-q25.1		DI-CMT A	Xp22.2	*PRPS1*	
19p12-p13.2	*DNM2*	DI-CMT B	・Mini fascicular型常染色体劣性		
1p34	*YARS*	DI-CMT C			
1q22	*MPZ*	DI-CMT 3	12q13.1	*DHH*	46XY gonadal dysgenesis
8p21	*NEFL*	CMT2E			
常染色体劣性			・Neuronopathy型常染色体優性		
8q21.1	*GDAP1*	CMT RIA			
			3q12-13		HMSN-P

あり，CMT全体の約50%，脱髄型の約70%を占める(図1)[3]．CMT1Aの原因はミエリン構成蛋白である*PMP22*(peripheral myelin protein 22)を含む染色体17p11.2の1.4Mbのゲノムの重複により起こる．HNPPは同じ領域のdeletionによりひき起こされる．厚生労働省研究班(祖父江班)における日本の全国集計では，*PMP22*重複と*GJB1*変異，*MPZ*変異は約6：2：2の割合で，日本では，欧米よりMPZ変異の割合が多い[4]．一方，山形大学の早坂らの検討では，*PMP22*の重複変異の割合が23.4%と少ない可能性があることが，未発表であるが報告されている．世界的には脱髄型で2番目に頻度の高いものはCMTX1である．本症はX染色体優性遺伝(XD)で，原因遺伝子は*GJB1*(gap junction protein, beta-1, Cx32)であり，本蛋白はミエリンと軸索間のgap junctionを形成し，栄養物質の交換にも関与する．その次にミエリン構成蛋白である接着能のある*MPZ*(myelin protein zero)，さらに*PMP22*のmutationと続く．Intermediate formでは*GJB1*の変異が多く，そのほかは少数でまだよくわかっていない．軸索型(CMT2)では*MFN2*，*GJB1*の順であり，その他の遺伝子は少数で，原因の同定できない症例も多い．他の遺伝子異常症は，頻度としては

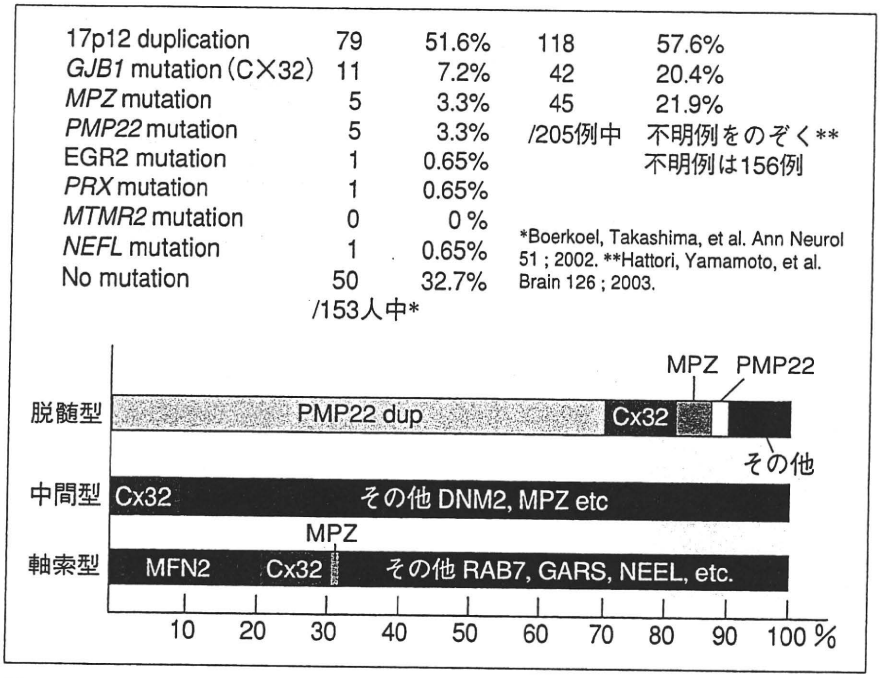

図1　CMTの遺伝子異常とその頻度(Szigeti, et al. NeuroMolecular Med 2006より改変引用)

おおよそ5％以下と推定される．

遺伝子検査法とその進歩

これまでに同定された遺伝子数の多さから原因遺伝子の同定は容易ではないが，CMT1Aのアスコルビン酸治療の臨床試験が世界的にも始まり，今後の治療への展望を考える上でも，その同定は必要となってくるであろう．上記のような遺伝子異常の頻度をふまえ，以下のような順序で遺伝子検査を行うのが効率的である．

まず，神経伝導検査で脱髄型の場合，これまでの報告では60～70％がCMT1Aであり，遺伝子診断として*PMP22*の重複についてはまずスクリーニングする必要がある．また，CMT全体でも半数はCMT1Aであるため，CMTの型がはっきりしない場合にはスクリーニングのはじめに，PMP22の重複を確認すべきと考えられる．一方，上肢のMCVが38m/secを超えるCMT1Aは，ほぼゼロであり[4]，明らかなCMT2にはPMP22の重複の検査は不要といえる．

このPMP22の重複を調べるためにさまざまな方法が考案，実施されている．わが国では，比較的高感度の方法であるFISH法を用いた検査が，三菱化学メディエンス社から提供されている．CMT1Aの原因はミエリン構成蛋白である*PMP22* (peripheral myelin protein 22)を含む染色体17p11.2の1.4Mbのゲノムの重複により起こる．また，HNPPは同じ領域のdeletionによりひき起こされる．FISH検査はCMT1A, HNPPともに検出可能で，その精度は高く染色体検査の1項目として保険適応となっている．*PMP22*の重複以外の遺伝子異常の検出には，アメリカなどではシークエンス解析による遺伝子変異の検出が，CMTの遺伝子検査としてAthena diagnostics社からコマーシャルベースで提供されている．一方，本邦では，数カ所の研究施設が研究の一環として行っているが，臨床検査としては提供されていない．そこで，われわれは厚生労働省の研究班の研究事業として検査法の確立を行っている最中である．

遺伝子変異の検索は，一般的にはシークエンス解析により行われ，比較的頻度の高い*GJB1*, *MPZ*, *PMP22*などの遺伝子がはじめに検査される．これらの三つの遺伝子は比較的小さくエクソンも少ないため，シークエンス解析は可能であり，いくつかの施設において無償で提供されてきた．しかしながら，現在までにさらに29以上の原因遺伝子が報告され，すべてをシークエンス解析で行うことは，1検体あたり少なくとも100万円以上(概算140万円)のコストと膨大な労

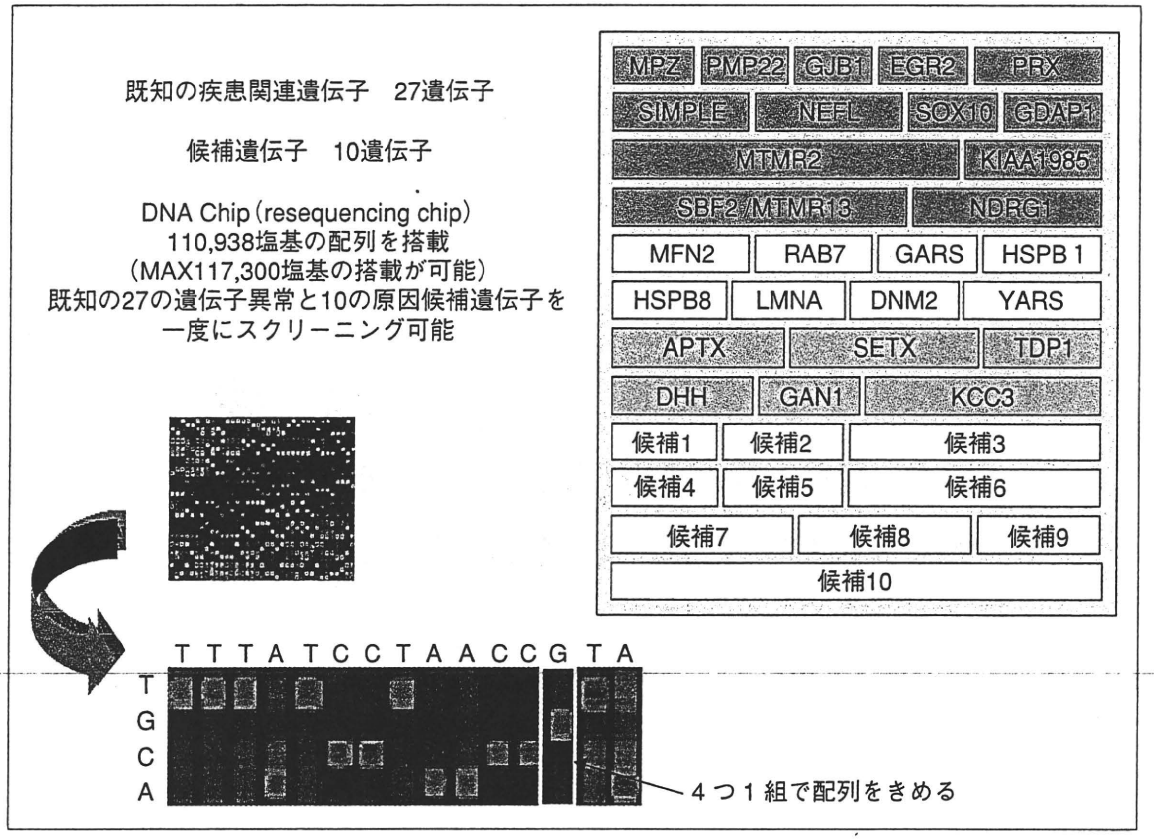

図2　遺伝性ニューロパチー遺伝子診断チップ〔Gene Chip image(100K array)〕

力を要するため，シークエンス法による網羅的な解析を行うことは困難であった．そこで，多数例の遺伝子異常を比較的高感度で調べる方法の一つにDHPLC(denaturing high-performance liquid chromatography)がある．これは，液体クロマトグラフィーと厳密な温度コントロール可能なオーブンと特殊なDNA分離カラムを組み合わせ，遺伝子異常を同定する方法である．加熱したPCR産物をゆっくり冷却することにより，正常配列のDNA断片と異常配列のDNA断片が混ざる形で形成されたヘテロデュプレックスを特殊カラムにかけ，遺伝子変異を検出する方法である．SSCP法やDGGE法などと原理は類似する部分もあるが，それらをより簡便に実施できるように設計され，高感度，ハイスループット，比較的低ランニングコストという特徴がある．本法でスクリーニングを行い，異常のみつかったPCR産物のみをシークエンス解析で調べることで変異が確定される．われわれの検討では，*MPZ*, *PMP22*, *GJB1*の変異はほぼ100%同定することが可能であった[5]．多くの遺伝子でも90%以上の感度は期待できると考えられる．DHPLC法の欠点は直接には配列が決定できない点である．また，遺伝子多型が含まれる領域はすべて異常と検出されるため，その領域についての異常の検出は困難であり，シークエンス解析を行わなければならない．DHPLC法はシークエンスの必要な検体を簡単に減らせられるという点で，現在も有用なスクリーニング法の一つである．

一方，近年の遺伝学の進歩により発見されるCMTの原因遺伝子数が増えるに従い，より網羅的で高速，低コストな方法が望まれるようになってきた．そこで，われわれが新しく取り組んだのは，マイクロアレイ技術を用いた革新的な遺伝子配列決定法でリシークエンスアレイ法を利用するものである．マイクロアレイ法の原理は，25～100塩基の配列の長さをもつプローブをマイクロチップ上に数千から200万個並べ，ラベルをしたDNA断片とハイブリダイゼーションし，その信号強度を高精度のスキャナーで読み取り，シークエンス配列を決定するものである．通常は，RNAの発現量解析，遺伝子のマッピング，遺伝子多型と疾患の関連解析，ゲノムのコピー数解析などに用いられるが，シークエンス解析

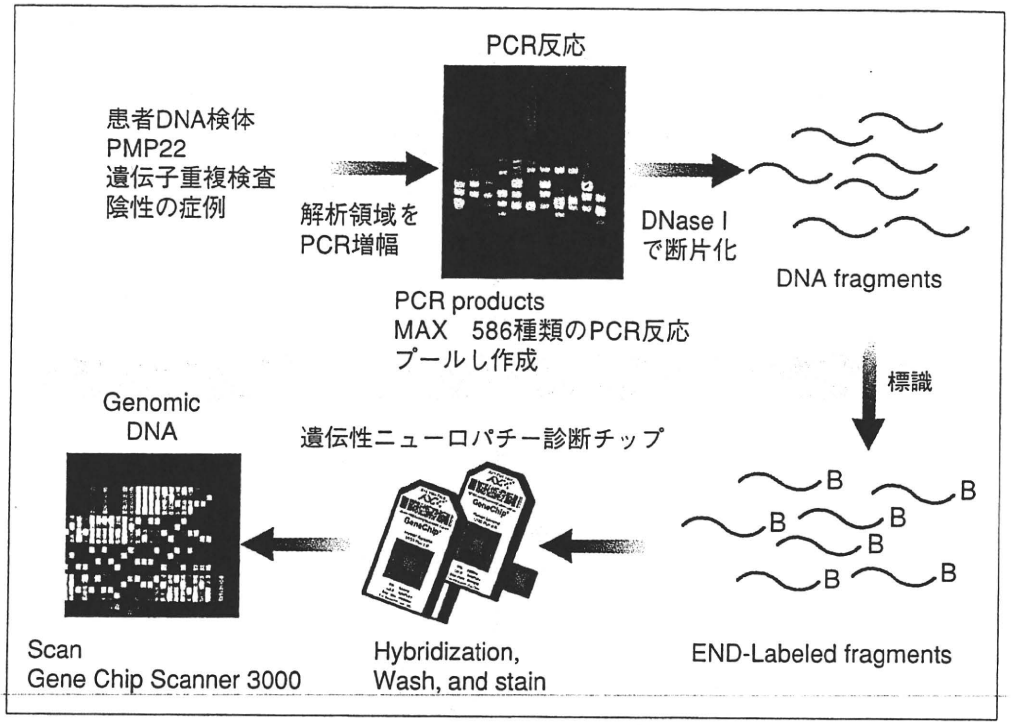

図3　遺伝性ニューロパチー遺伝子診断システム

にも用いられるようになった．われわれの用いるDNAチップには，25塩基のDNAオリゴの中央部(13塩基目)をA, C, G, T の4つに変えたものをひとかたまりとし，それを一塩基ずつずらすことにより，配列を読み取るというものである(図2)．このDNAアレイにチップ上に乗せた遺伝子を多くのプライマーセットを用い，PCRで増幅した後にラベルし，ハイブリダイゼーションが行われる．そのチップをスキャンし，コンピューター解析することで遺伝子配列を決定することができる(図3)．実際，本法により網羅的なCMT遺伝子診断が現実的なものとなった．弱点としては，シークエンス解析に比べ，欠失や挿入の変異の検出が難しいことである．さまざまな遺伝子異常があるため，その異常の検出を単独で100%検出する方法はないので，コストを考慮しながらいくつかの方法を組み合わせることが必要であろう．

われわれのCMT遺伝子診断用DNAチップには，CMTおよびその類縁疾患の原因27遺伝子を搭載した(図2)．本チップは，通常のシークエンス法では，1例あたり約140万円のコストがかかるところを7万円に圧縮し，実際の研究レベルでの遺伝子検査ができるようになった．現在，当科において本チップによるCMTの遺伝子診断を受けつけている．今後多くの遺伝子異常が同定され，臨床像と遺伝子異常との関連が明らかになるであろう．また，本遺伝子チップに新規の候補遺伝子を載せることにより新しい原因遺伝子の発見も可能となる．

CMT診断の全体の検査の流れの案として図4に示した．CMTの場合はまず，家系調査，詳細な鑑別診断，神経伝導検査が必須である．もっとも鑑別が重要となる疾患はCIDPと思われるが，それについては，可能な限り臨床的に突き詰めるべきであろう．その理由は，遺伝子診断に時間を要すること，および遺伝子診断陰性例がCMTではないとはいいきれないこと，さらに多くのCIDP例にまで遺伝子検査を調べる余裕が通常の研究室にはないためである．しかし，長期に慢性進行性に経過するCIDP症例についてはCMTの可能性があるため，遺伝子診断が有用な場合もあると思われ，その場合の遺伝子検査は有用であろう．また，遺伝子検査は万能ではないため，他のニューロパチーとの鑑別も含めて神経生検の所見も重要と考えられる．遺伝子検査全般にいえることであるが，診断結果の判定には，未報告の新規の遺伝子変異の場合，それまでの同

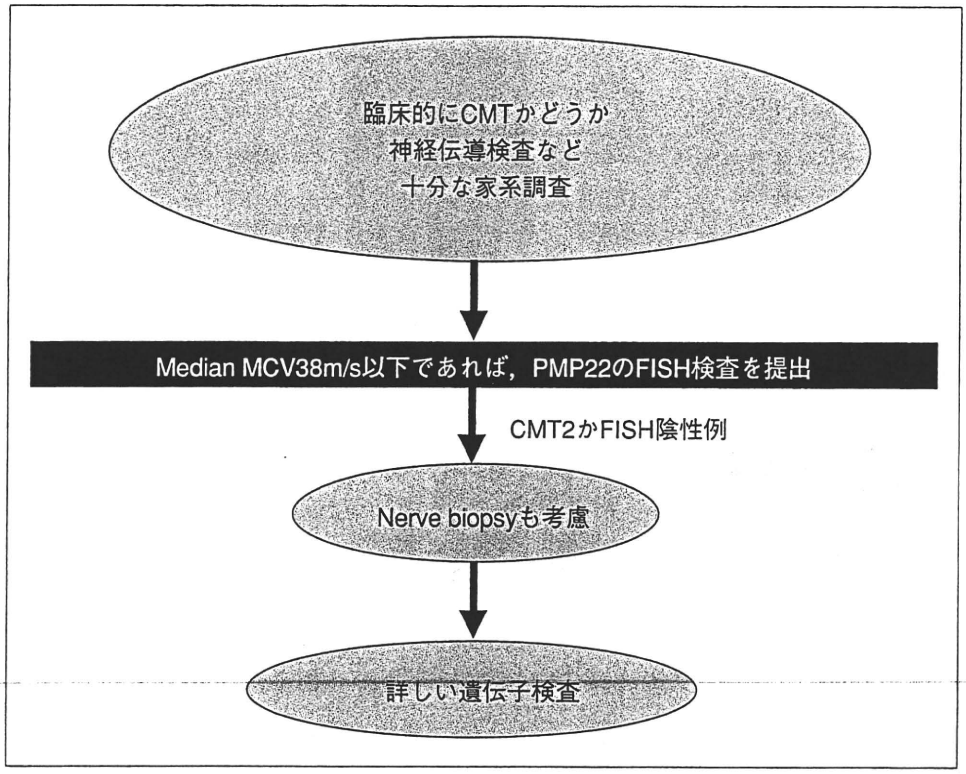

図4　CMTの診療の流れ

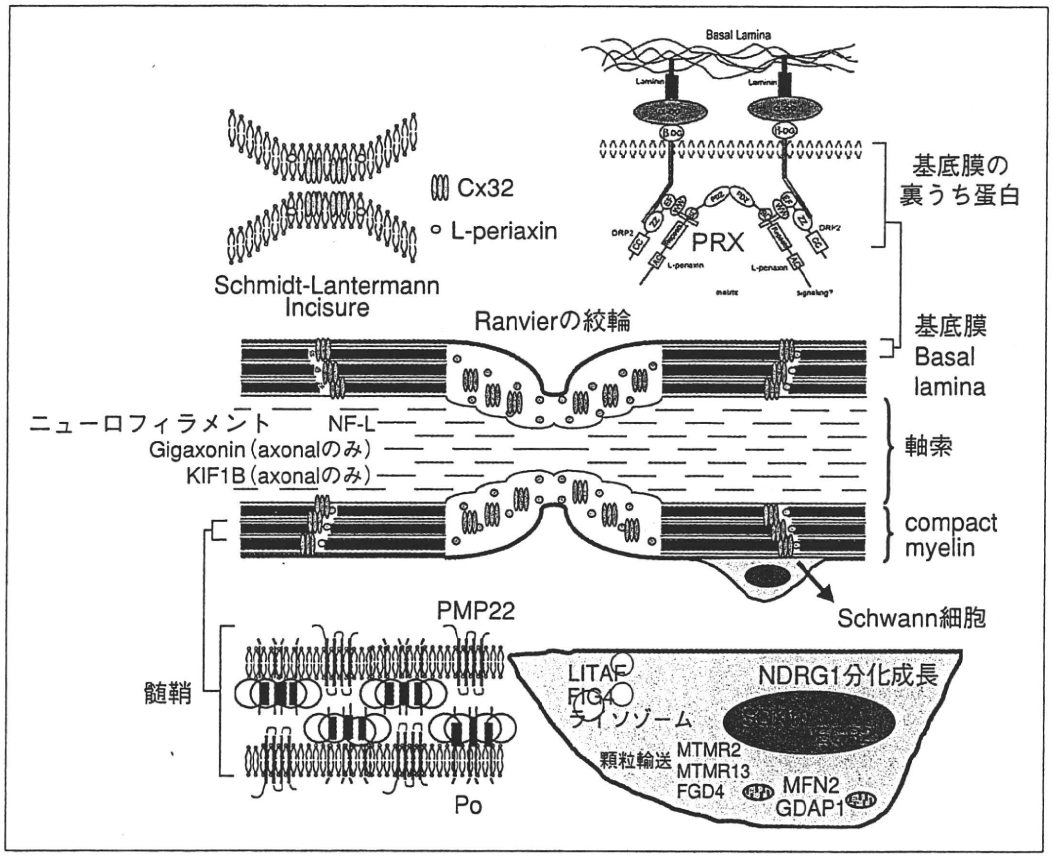

図5　脱髄型CMTの原因遺伝子

じ遺伝子に異常をもつ報告例との臨床像の比較，さらにその家系での遺伝子検査で遺伝子変異の伝達に矛盾がないことの確認(segregation study)，コントロールには同一の異常がないことの確認

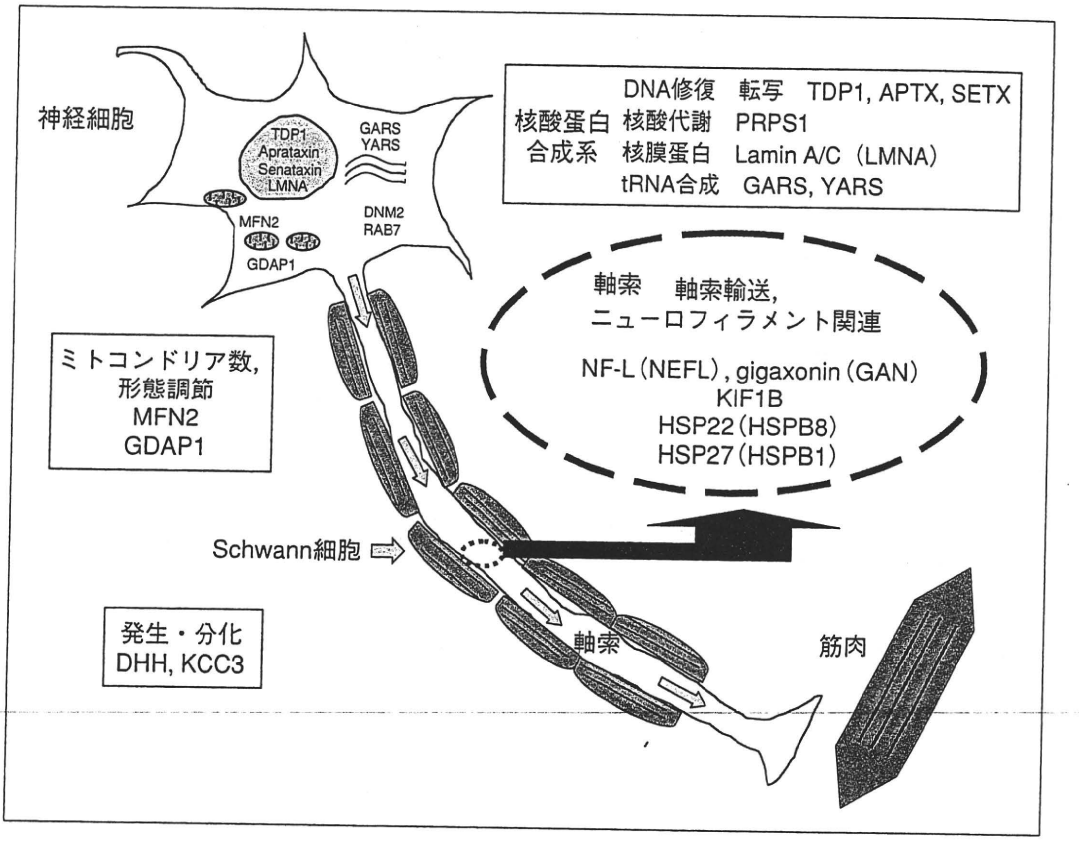

図6　軸索型CMTの原因遺伝子

が必要である．そのため，臨床的にCMTの臨床像ではなくニューロパチーがあるというだけの場合には，遺伝子検査の結果の判定は難しいことも多い．

CMTの遺伝子異常と病型

図5に脱髄型の病態を，図6に軸索型の病態をシェーマに示した．現在までに原因遺伝子が明らかにされた病型について概説する．

1．常染色体優性遺伝形式の脱髄型CMT（CMT1）

脱髄型CMTの原因として，現在までに6つの遺伝子異常が報告されており，CMTの患者数がもっとも多い病型である．

a．CMT1A　Peripheral myelin protein 22（*PMP22* duplication）

CMT1Aの原因として，*PMP22*を含む17p11.2の1.4Mbのゲノムの重複が原因で，PMP22の発現量が増加することにより疾患がひき起こされる．本邦の報告では，平均発症年齢20.3歳で，約60％は20歳以下で発症する．下肢遠位部からの筋力低下が緩やかに進行するが，臨床型には個人差が大きい．上肢のMCVが17～27m/secのときには，本症の可能性が高い．また，PMP22のアミノ酸置換もCMTやDSSの原因となりうる．アスコルビン酸によりPMP22の発現量が低下するため，その治療が試みられている．

b．CMT1B　Po（*MPZ*）

MPZもミエリン構成蛋白で，ミエリンの構成成分の50％を占める．コンパクトミエリンの各層の接着を行い，それ自身がミエリン構造を形成する．*MPZ*の異常はCMT1，DSS，CHN，CMT2などさまざまな臨床型をもひき起こすことが特徴で，神経伝導検査が10～20m/secと明らかに遅延する病型と40m/sec以上のCMT2I，CMT2Jの病型を示す群がある[6]．

c．CMT1C（*LITAF*，*SIMPLE*）

CMT1Cの原因である*SIMPLE*（small integral membrane protein of lysosome/late endosome）または別名*LITAF*（lipopoly saccharide-induced tumor necrosis factor-alpha factor）の機能は不明であるが，ubiquitin mediated lysosomal degradationと関連していると推定されている．臨床的には遠位部優位の筋萎縮と感覚の低下がみられる．MCVは16～25m/secでtemporal dispersionや

conduction blockを認める．神経生検ではオニオンバルブ形成を認める[7]．

d．CMT1D　Early growth response 2（*EGR2*）

*EGR2*はミエリン形成時に必要な転写因子で，*PMP22*や*MPZ, GJB1, PRX*などの遺伝子発現をコントロールしている．EGR2の異常では，表現形はDSSやCHNなど重症型が多い．

e．CMT1F　Neurofilament light chain（*NEFL*）

*NEFL*の異常では，ニューロフィラメント形成に関与するため，はじめは軸索障害型のCMT2Fの原因として報告された．しかし，その後の報告では，神経伝導速度が15～38m/secの例やオニオンバルブをもつ例の報告などがあり，軸索障害型よりも脱髄型をより多く示すことが示された．臨床型は多様であり，早期発症例から軽症例までにわたる．通常優性遺伝形式のNEFLの点変異で発症するが，近年ナンセンス変異のホモ接合体が報告された[8]．

その他，優性遺伝性の脱髄型CMTには，転写因子の*SOX10*（SRY-BOX 10）や8p23に連鎖するHMSNの臨床像を呈さない神経伝導速度の異常と菲薄化ミエリンを主に示す家系において，*ARHGEF10*（Rho guanine-nucleotide exchange factor 10）が原因として同定されている．

2．常染色体劣性遺伝形式の脱髄型CMT（CMT4）

CMT4の病態としては，ほとんどが原因遺伝子・蛋白のloss-of-functionであり，ミエリンの構成蛋白，分化成長因子などで10の原因が明らかにされている．また，それとは別に*EGR2, PMP22, MPZ*などの単独でも優性遺伝のCMTの原因になる遺伝子異常のホモ接合体もみつかっており，その場合はより重症な臨床型を示すことが多い．日本人の症例としては*GDAP1, SBF2/MTMR13, PRX*の異常症が確認されている．

a．CMT4A　Ganglioside-induced differentiation-associated protein 1（*GDAP1*）

CMT4Aの原因はCMT2Kと同じ*GDAP1*の異常である．本症は，発症の早いDSSの臨床像をとることも多く，嗄声を伴う．上肢の神経伝導検査では25～35m/secと報告され，腓腹神経は神経脱落も多く，オニオンバルブ形成もみられる．GDAP1の機能は，ミトコンドリアの分裂と関連し，患者の細胞でミトコンドリア体積の増加や呼吸鎖の活性の低下が報告されている．CMT2A2の原因であるMFN2とともに働いて，ミトコンドリア分裂や融合を調節し，ミトコンドリアの数や容積などの調節にかかわっていることが示されてきている．

b．CMT4B1　Myotubularin related protein 2（*MTMR2*）

c．CMT4B2　SET binding factor 2（*SBF2 / MTMR13*）

Excessive myelin foldingを特徴とするCMT4B1の原因として*MTMR2*（myotubularin related protein 2）が報告され[9]，発症は，2歳前後で神経伝導検査は9～20m/secである．この蛋白はphosphatase活性をもつ．

緑内障を伴うCMT4B2の原因として*SBF2*（SET binding factor 2）*/MTMR13*[10]が同定された．SBF2/MTMR13はmyotubularin蛋白の一つであるが，CMT4B1の原因であるMTMR2とCMT4B2の原因であるSBF2/MTMR13が4量体を形成し，phosphatase活性を数十倍に高めることがわかってきた．この二つの蛋白が複合体として働くことが，両蛋白の異常症が類似の臨床像を示す理由であると考えられる．本症の機序は，リン酸化イノシトールの代謝の脱リン酸化とかかわることで，Schwann細胞のvesicular traffickingを調節していると推定されている．

d．CMT4C　SH3TC2（*KIAA1985*）

CMT4Cの原因としてSH3TC2（*KIAA1985*）が[11]報告されている．機能はよくわかっていない．今までの報告では，幼小児期発症のニューロパチーで早期に側彎となり，呼吸筋も障害される．しかし本症においては，同一家系内でも臨床像に大きな違いがみられることも多い．上肢の伝導検査では，MCVが10～34m/sec以下でオニオンバルブ形成，tomaculaおよびgiant axonなどが報告されている．

e．CMT4D　HMSN-Lom（*NDRG1*）

ブルガリアのローム地方に住むGypsieにおいて，報告されている難聴を伴うHMSNの原因として*NDRG1*（N-myc downstream regulated gene 1）が報告された．MCVは9～20m/secで，かなり遅い．*NDRG1*は末梢神経の成長や分化にかかわると考えられている．